Supporting Information

Separator-Free Aqueous Zinc-Iodine Batteries: An In-Situ Dual-Confinement Interface Enabling Electrostatic Reversible Polyiodide Capture/Release

Yamei Liu[1], Xiaofan Tian[1], Lu Wang[1], Lijin Xie[1], Zhenchao Li[1], Yuxin Ge[1], Zhao Li,[4] Zhongchao Bai[3], Huakun Liu[3], Nana Wang[2,], Guoxiu Wang[2], Xiaochuan Ren[1,]**

[1]Institute of Materials for Energy and Environment, College of Textiles & Clothing, School of Materials Science and Engineering, Qingdao University, Qingdao 266071, China. Email: rxchuan@qdu.edu.cn

[2]Centre for Clean Energy Technology, School of Mathematical and Physical Sciences, Faculty of Science, University of Technology Sydney, Sydney, NSW 2007, Australia. Email: Nana.Wang@uts.edu.au

[3]Institute of Energy Materials Science, University of Shanghai for Science and Technology, Shanghai, 200093, China

[4]Department of Materials, Imperial College London, London SW7 2AZ, United Kingdom

*Correspondence email: rxchuan@qdu.edu.cn, Nana.Wang@uts.edu.au

1. Experimental section

1.1 Materials

1,4-benzenedicarboxylic acid (BDC, 99%) and triethylamine (TEA, 99%) were purchased from Aladdin Biochemical Technology Co., Ltd. and used as received. Nickel(II) chloride hexahydrate ($NiCl_2 \cdot 6H_2O$, 99%) and Zinc iodide (ZnI_2, 98%) were purchased from Shanghai Macklin Biochemical Technology Co., Ltd. and used as received. Iodine (I_2), potassium iodide (KI), N, N-dimethylformamide (DMF), anhydrous ethanol, and 1-Methyl-2-pyrrolidinone (NMP, 99%) were purchased from Sinopharm Chemical Reagent Co., Ltd. and used as received. Active carbon (AC) was purchased from Kuraray Co., Ltd. CNF aqueous gel with a solid content of 1.7 wt% was produced by Zhejiang Jinjiahao Green Nanocellulose Co., Ltd, in which the CNFs are 1-50 nm in diameter and 1-30 μm in length.

1.2 Synthesis of Ni-MOF nanosheets

32 mL DMF, 2 mL anhydrous ethanol, and 2 mL deionized water were first mixed in a 100 mL glass bottle. Then, 0.75 mmol BDC and 0.75 mmol $NiCl_2 \cdot 6H_2O$ were added to the bottle, respectively. After the solution was stirred for 5 minutes, 0.8 mL TEA was injected into the solution. Then, the glass bottle was ultrasonicated continuously for 4 hours under ambient conditions. Finally, the products were collected via vacuum filtration, washed for 4 times with ethanol, and dried in a vacuum oven.

1.3 Fabrication of NCNF@Zn, NCNF separator and CNF@Zn

NCNF@Zn was synthesized via a simple two-step process, including physically mixing and dehydration. Briefly, 17 mg Ni-MOF was dispersed in 15 mL NMP and then sonicated for 1 h to obtain a homogeneously dispersed solution. Then, 7 g CNF

solution (solid content ~1.7%) and 10% PVDF were added. After vigorous stirring at room temperature for 2 h, the dispersion was coated on the surface of zinc metal. The zinc metal was then transferred to an oven at 50℃ and held for 48 hours to obtain the NCNF@Zn. The NCNF separator can be prepared by pouring the above dispersion directly into a glass petri dish and then drying it. For comparison, the CNF@Zn was prepared without Ni-MOF under the same conditions.

1.4 Synthesis of I_2@AC composite

The I_2@AC composite was prepared by an I_2 sublimation method. In detail, AC and I_2 in a weight ratio of 1:2 were mixed thoroughly by grinding for 10 min. Then the mixed material was transferred into a Teflon-lined autoclave and heated at 95℃ for 6 h. Subsequently, the Teflon liner was unsealed and further heated at 130°C for 5 h to eliminate the unstable iodine from the carbon materials. Upon cooling, the I_2@AC was obtained.

1.5 Materials characterization

X-ray diffraction tests were implemented on a diffractometer with Cu Kα radiation (XRD, Rigaku, Ultima IV; Cu Kα radiation λ = 0.15418 nm). The scanning electron microscopy (SEM; JEOL, JSM-7800F) and transmission electron microscopy (TEM; JEOL, JEM-2100plus) were used to study the micro-morphologies of samples. Static contact angles were obtained using a JY-PHb contact angle measuring device. X-ray photoelectron spectroscopy (XPS; Kratos, AXIS-ULTRA, DLD-600 W) and Fourier transform infrared spectroscopy (FTIR; TERMO, IS10) characterizations were used to investigate the surface chemistry state. Raman spectra were tested on LabRam HR Evolution. UV-vis spectra were obtained on a Shimadzu UV-Visible spectrophotometer (UV-3600i Plus). The simultaneous thermal analyzer (TG; METTLER TOLEDO) was

used to analyze changes in material quality. The nitrogen adsorption-desorption measurements were conducted at 77 K with BSD-PMC2. Specific surface area and pore size distribution were calculated using the Brunauer-Emmett-Teller (BET) theory. The static diffusion tests of polyiodides were conducted using the H-type electrolytic cells, in which 10 mM I_3^- solution and deionized water are added to the left and right chambers, and the two chambers were separated by GF and NCNF, respectively. The 10 mM I_3^- solution was prepared by dissolving 10 mM I_2 into 0.1 M KI aqueous solution. The ionic conductivity (σ) and MacMullin number (N_M) were calculated by the following equations:[1]

$$\sigma = \frac{d}{R \cdot S} \#(1)$$

$$N_m = \frac{\sigma_0}{\sigma_i} \#(2)$$

Where d is the thickness of the separator, R is the resistance based on the EIS test, and S is the surface area. σ_0 represents the ionic conductivity of the pristine 2M $ZnSO_4$ electrolyte at room temperature, while σ_i represents the ionic conductivity of the NCNF film soaked with the electrolyte under the same conditions.

1.6 Electrochemical measurements

Electrochemical measurements were carried out using 2025 coin-type cell. The separator-free symmetric cells (NCNF@Zn//Zn) were assembled by NCNF@Zn and Zn plate. The I_2 cathode was prepared by mixing 80 wt% active materials (I_2@AC), 10 wt% acetylene black, and 10 wt% PVDF binder in NMP solvent, of which the slurry was uniformly coated on a piece of carbon paper and subsequently dried at 45°C under vacuum overnight. The electrode was punched into disks with an approximate mass

loading of 0.8-1.2 mg cm^{-2} of the I_2.

The iodine cathode with ultra-high loading was prepared using the solution adsorption method. Specifically, I_2 and AC were dispersed in deionized water with a mass ratio of 1:1. Subsequently, carbon nanotubes and bacterial cellulose (BC) were added to the solution, accounting for 10% of the total electrode mass. Following ultrasonication and vacuum filtration, a free-standing film was formed. After overnight drying, the iodine content in the resulting electrode accounts for approximately 45 wt% of the total mass. Finally, the free-standing iodine cathode was punched into circular discs with an iodine loading of 20-22 mg cm^{-2}. Zn-I_2 full cells were assembled with Zn foil anode, glass fiber (GF) and I_2 cathode. However, NCNF@Zn-I_2 full cells were assembled by NCNF@Zn and I_2 cathode without separator. 2 M $ZnSO_4$ aqueous solution was employed as the electrolyte. Galvanostatic cycling tests were conducted at a potential range of 0.6-1.6 V (vs. Zn^{2+}/Zn) based on the Neware battery testing system (CT-4008T). In this work, the specific capacity of Zn-I_2 batteries was calculated based on the I_2 mass.

Electrochemical measurements, including linear sweep voltammetry (LSV), chronoamperometry (CA), and linear polarization (LP) curves, were conducted using an electrochemical workstation CHI660E (Chenhua Instrument Company, Shanghai, China). LSV and LP tests were measured in the three-electrode system, utilizing Zn foil or NCNF@Zn as the working electrode, a Pt plate as the counter electrode, and an Ag/AgCl electrode as the reference electrode. LSV measurements were carried out at a scan rate of 1 mVs^{-1}. LP tests were measured between -1.25 V and -0.7 V at 1.0 mV s^{-1}. The CA tests were measured at a fixed polarization potential of -150 mV. Electrochemical impedance spectra (EIS) tests were conducted over a frequency range of 0.01Hz to 100 kHz. DRT analysis was performed using DRTtools.[2, 3]

1.7 Flexible separator-free I_2||NCNF@Zn pouch cell

2 M $ZnSO_4$ was used as an electrolyte for I_2||NCNF@Zn pouch cell. The low-loading cathode was prepared by mixing as-prepared I_2@AC, acetylene black, and PVDF with a weight ratio of 8:1:1 in NMP. After drying, the weight of I_2 was around 1 mg cm^{-2}. For high-loading iodine cathodes, synthesized using the above solution adsorption method, the iodine loading is approximately 10-12 mg cm^{-2}. One piece of the above cathode was put on top of one piece of NCNF@Zn. The useful area of the low-loading pouch cell cathode is 6 cm^2, while that of the high-loading pouch cell cathode is 4 cm^2. No traditional separator was employed. The whole device was then sealed with aluminum laminated film, and the electrolyte was added at the same time.

1.8 DFT Calculations

The Vienna ab initio simulation package (VASP) was utilized to conduct density functional theory (DFT) computations employing the plane-wave method.[4, 5] The exchange-correlation interactions were delineated utilizing the generalized gradient approximation (GGA) implemented by the Perdew-Burke-Ernzerhof (PBE) functional.[6] The nuclear and electron interaction is described using the projected augmented wave (PAW) method.[7, 8] A plane wave basis set with an energy cutoff of 450 eV was employed to describe the valence electronic states. Geometry optimization was considered converged when the force variation fell below 0.03 eV/Å, while the self-consistent convergence of electronic energies was determined by an energy fluctuation threshold of less than 10^{-5} eV. A 15 Å vacuum layer was introduced along the b-direction of Ni-MOF and c-direction of Zn metal to avert interactions between periodic pictures. Dispersion interactions were accounted for using Grimme's DFT-D3 approach.[9] The adsorption energies ΔE were defined as follows:

$$\Delta E = E_{\frac{ads}{sub}} - E_{ads} - E_{sub} \#(3)$$

Where $E_{ads/sub}$ is the total energy of adsorbate-substrate, E_{ads} and E_{sub} are the energies of the adsorbate and substrate, respectively.

The desolvation energies of the Zn^{2+} were calculated using the following equations:

$$\Delta G = G[Zn(H_2O)_{x-1}] + G(H_2O) - G[Zn(H_2O)_x] \quad (4)$$

The Gibbs free energy of reaction species is derived as follows:

$$\Delta G = E_{ads}(H) + \Delta E_{ZPE} - T\Delta S \quad (5)$$

where ΔE_{ZPE} and ΔS are the changes in zero-point energy and entropy, respectively.

2. Supporting Figures

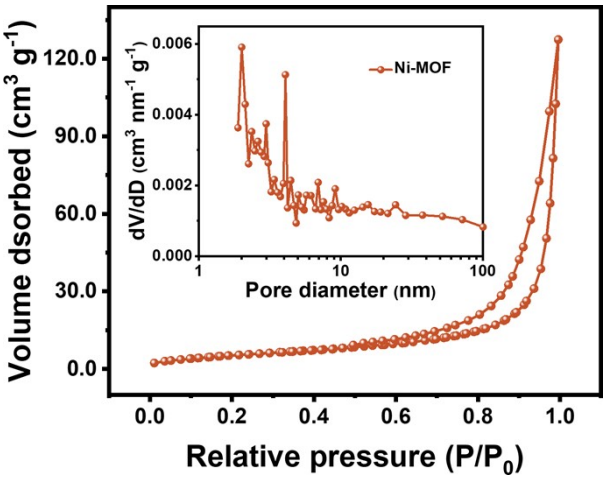

Figure S1. N_2 adsorption-desorption isotherms (inset is the pore size distribution plot) of Ni-MOF.

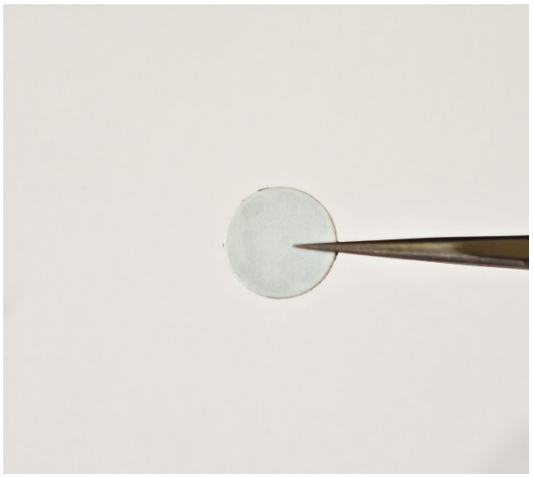

Figure S2. Optical image of the as-prepared NCNF@Zn.

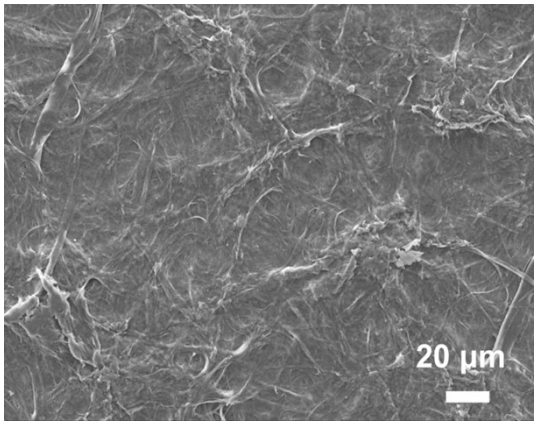

Figure S3. The SEM image of CNF@Zn.

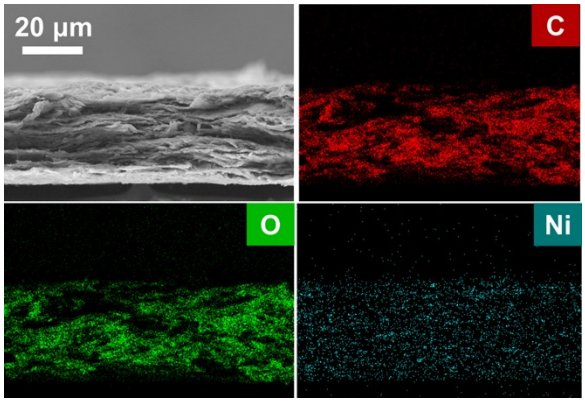

Figure S4. The cross-sectional SEM image and corresponding elemental mapping images of the as-prepared NCNF membrane.

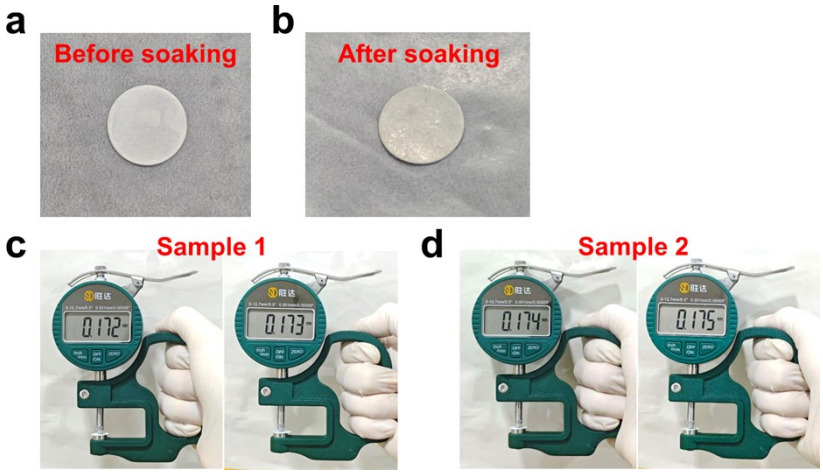

Figure S5. a-b) Optical images of NCNF@Zn before and after soaking in electrolyte. c-d) Thickness changes of two parallel NCNF@Zn samples before (left) and after (right) soaking.

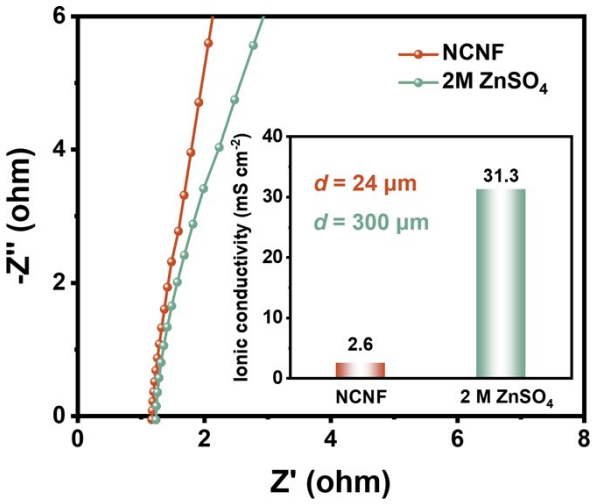

Figure S6. The EIS plots of NCNF film and 2M $ZnSO_4$ electrolyte, the inset shows the calculated ionic conductivity.

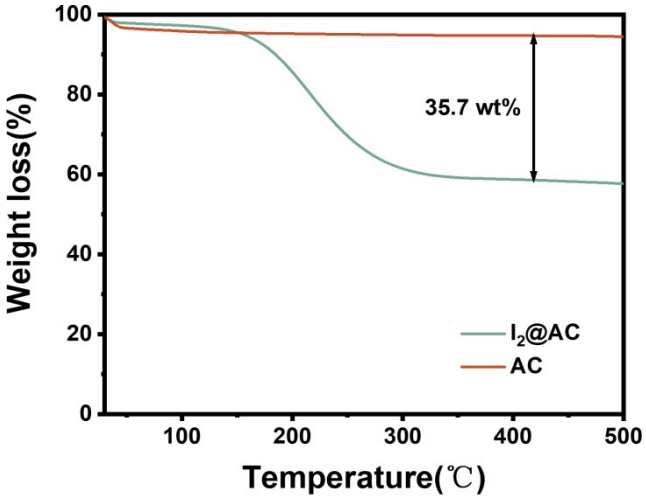

Figure S7. Thermogravimetric (TG) curves of I_2@AC and AC samples.

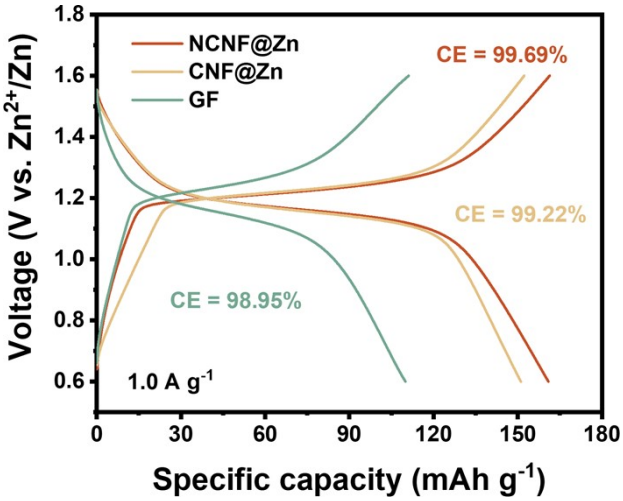

Figure S8. The 8th cycle of GCD profiles of the separator-free Zn-I_2 battery with NCNF@Zn, CNF@Zn and GF separator-based battery at 1.0 A g^{-1}.

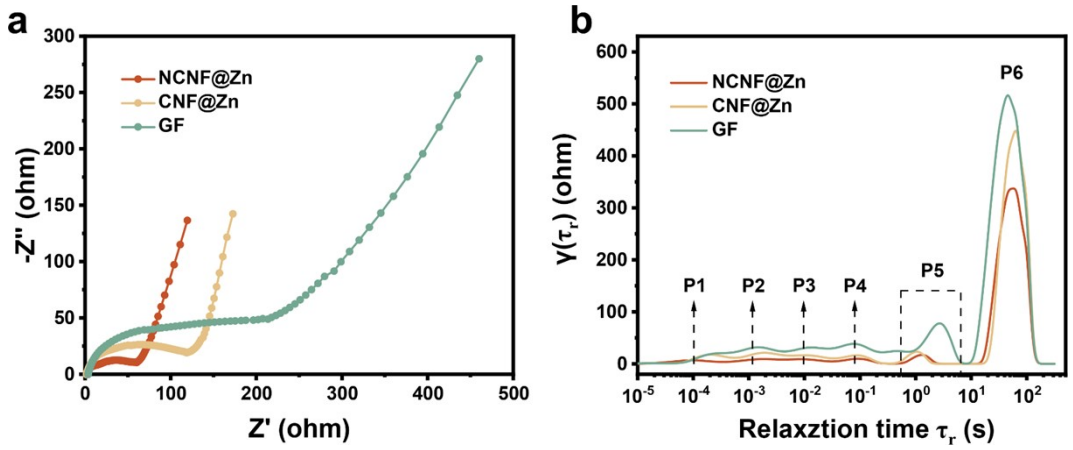

Figure S9. a) EIS plots and b) corresponding distribution of relaxation time (DRT) of separator-free NCNF@Zn, separator-free CNF@Zn, and GF separator-based batteries at the fully charged state.

P1: relaxation of electrons.

P2: desolvation of $Zn(H_2O)_6^{2-}$ at the electrode interface.

P3: Zn^{2+} migration and crystallization on the electrode surface.

P4: redox charge transfer reactions.

P5: interfacial charge exchange/electrolyte mass transport processes.

P6: ion diffusion.

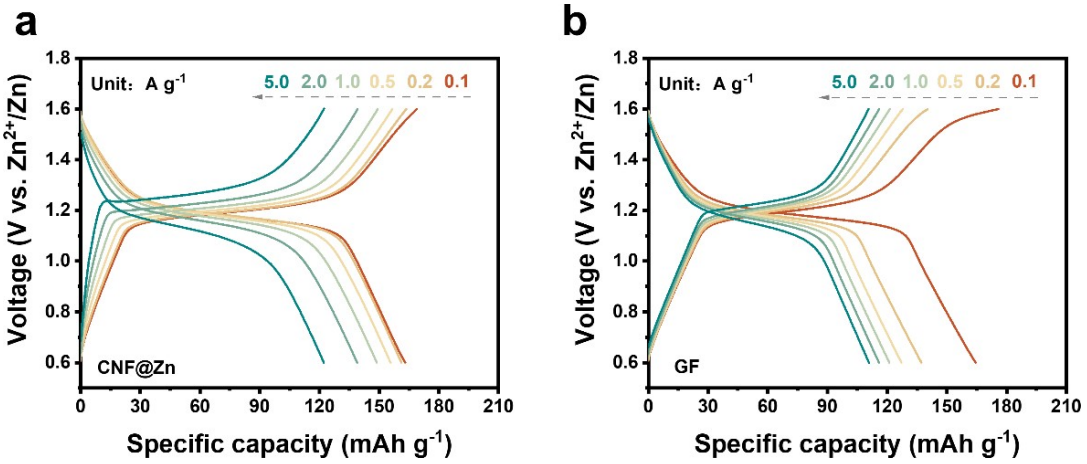

Figure S10. GCD profiles of a) separator-free CNF@Zn battery and b) GF-based battery at different current densities.

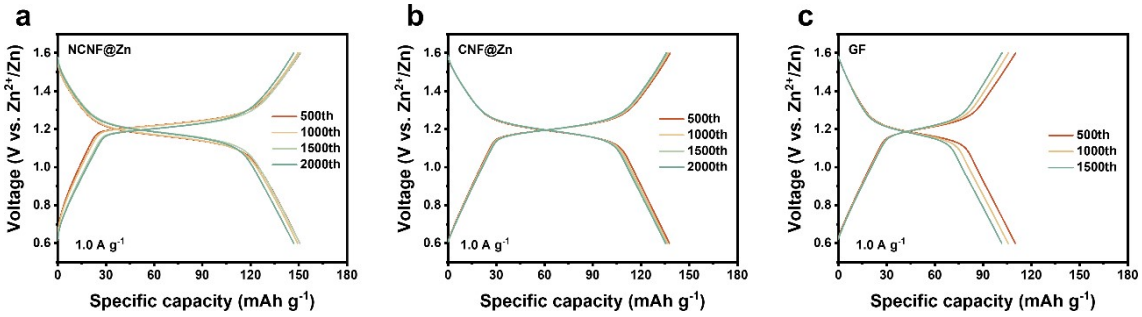

Figure S11. Selected GCD profiles of Zn-I_2 batteries with a) NCNF@Zn, b) CNF@Zn, and c) bare Zn with GF separator at 1.0 A g^{-1}.

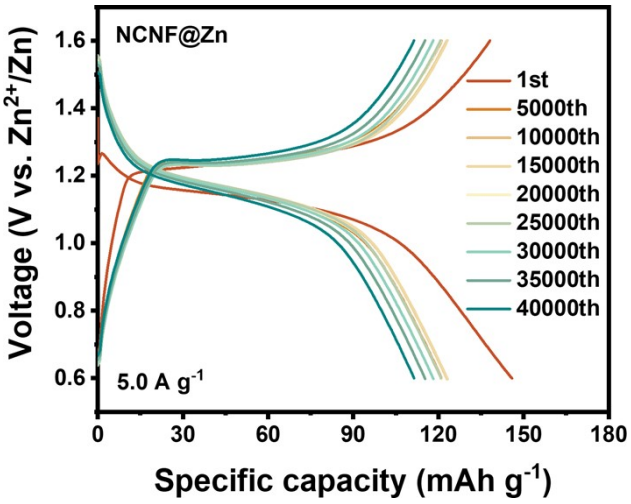

Figure S12. Selected GCD profiles of the separator-free Zn-I_2 battery with NCNF@Zn at 5.0 A g^{-1}.

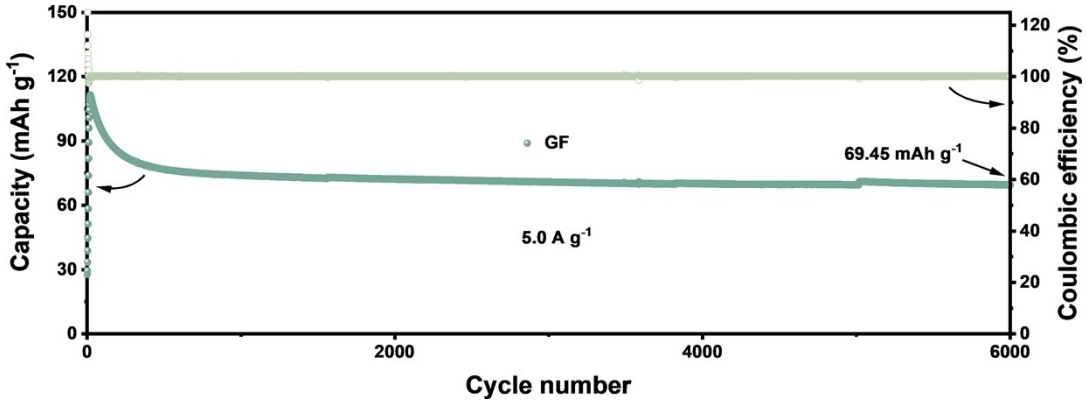

Figure S13. The cycling performance of the GF-based battery at 5.0 A g^{-1}.

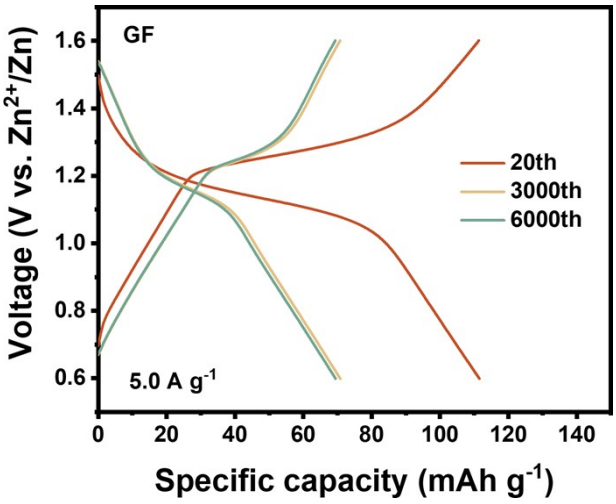

Figure S14. Selected GCD profiles of Zn-I_2 batteries with GF separator at 5.0 A g^{-1}.

Figure S15. Time-dependent visualization experiments of polyiodide shuttling in H-type cells with NCNF, CNF and GF separators.

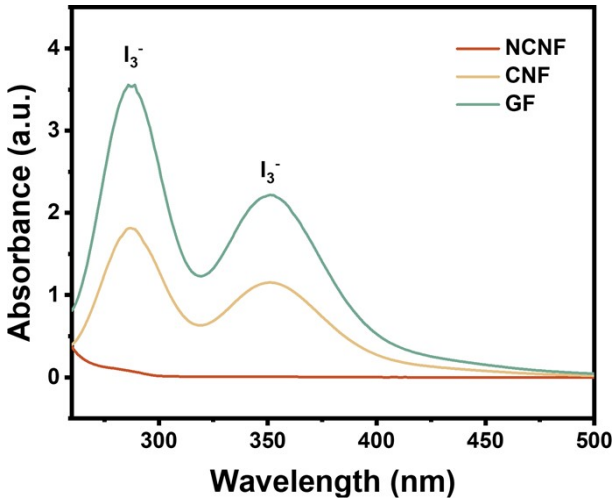

Figure S16. Corresponding UV-vis spectra of the right-side solutions in H-type cells with NCNF, CNF and GF separators after 2 h.

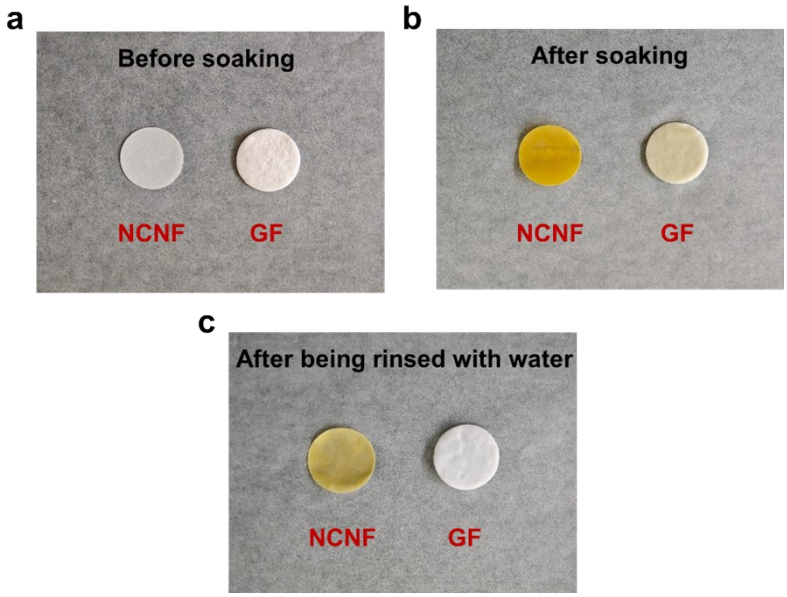

Figure S17. The photos of NCNF and GF separators a) before soaking, b) after soaking, and c) after being rinsed with water.

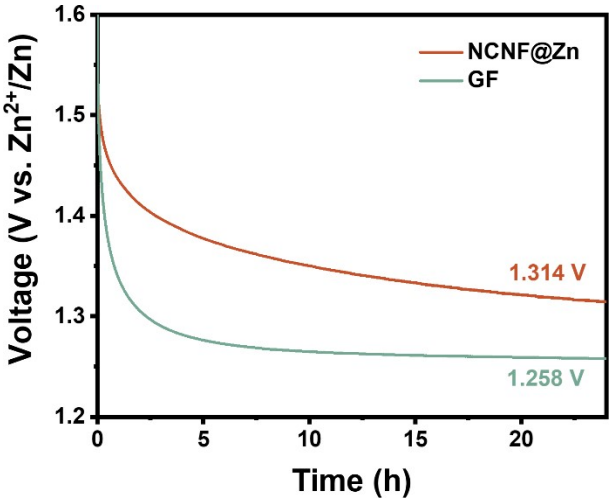

Figure S18. Self-discharging profiles of the separator-free Zn-I_2 cell with NCNF@Zn and the GF-based Zn-I_2 battery.

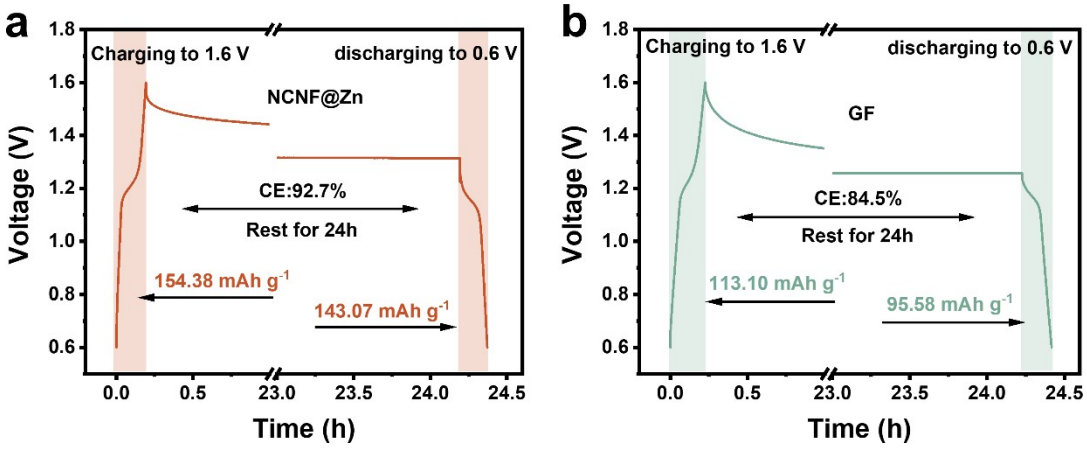

Figure S19. Self-discharge performance of a) the separator-free Zn-I_2 battery with NCNF@Zn and b) the GF separator-based battery.

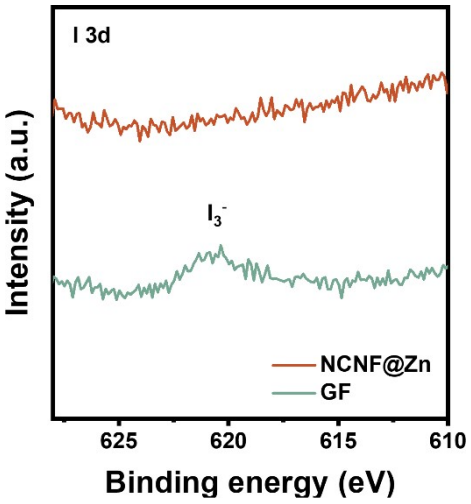

Figure S20. I 3d high-resolution XPS spectra of NCNF@Zn (the NCNF layer was torn off) and bare Zn anode after 50 cycles at 1 A g^{-1}.

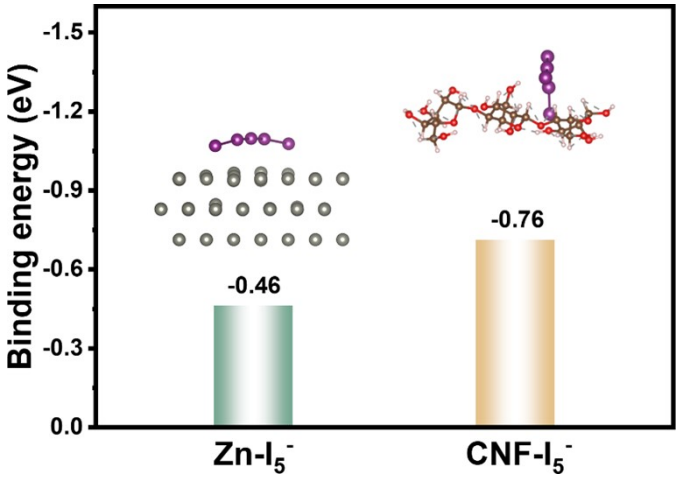

Figure S21. Computational binding energies of I_5^- with the Zn metal and CNF (inset of the corresponding calculation models).

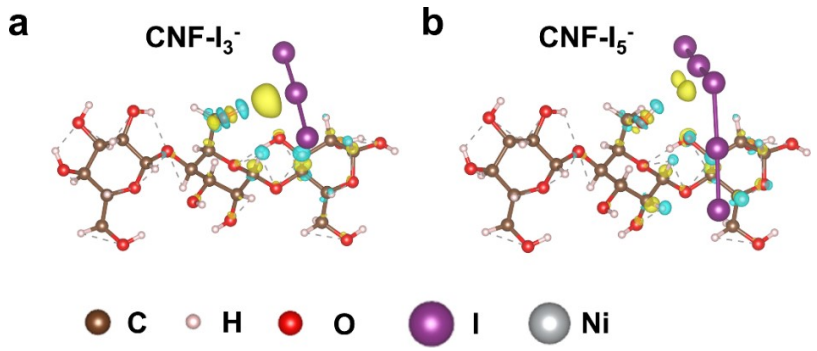

Figure S22. Differential charge density distributions of a) I_3^- and b) I_5^- with CNF (yellow and blue colors represent charge accumulation and depletion regions, respectively).

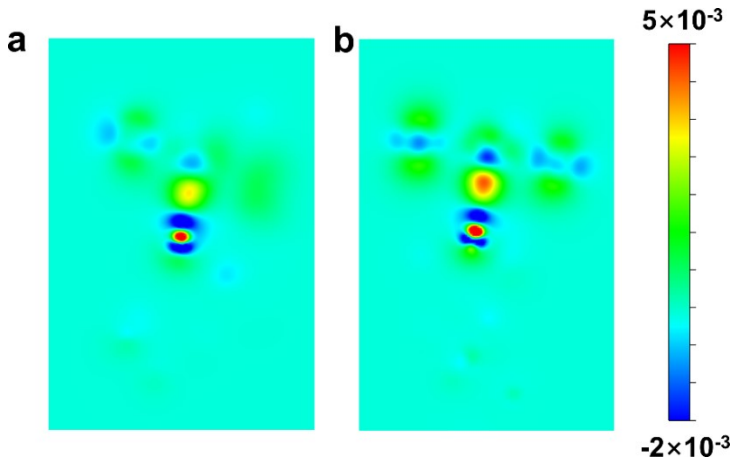

Figure S23. Two-dimensional charge density difference slice contours for I_3^- adsorption on a) CNF and b) NCNF surfaces.

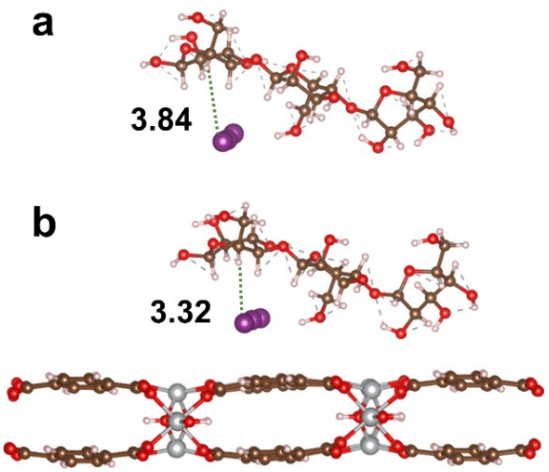

Figure S24. The optimized structural models of I_3^- with a) CNF and b) NCNF.

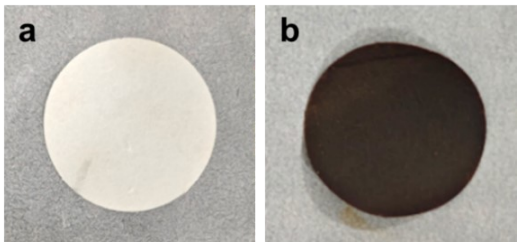

Figure S25. The photos of the freestanding NCNF membrane a) before I_3^- saturated adsorption and b) after I_3^- saturated adsorption.

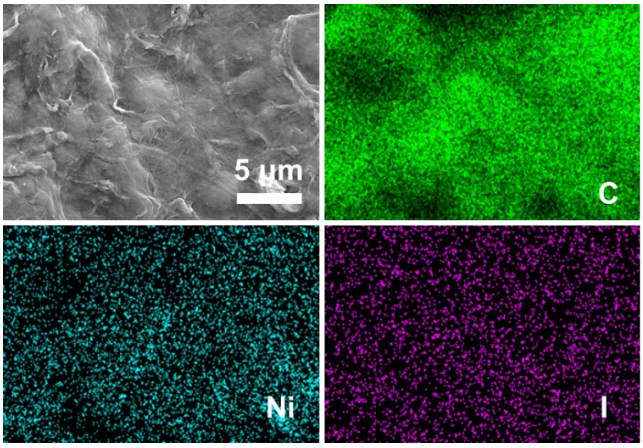

Figure S26. SEM and corresponding elemental mapping images of NCNF membrane saturated with I_3^-.

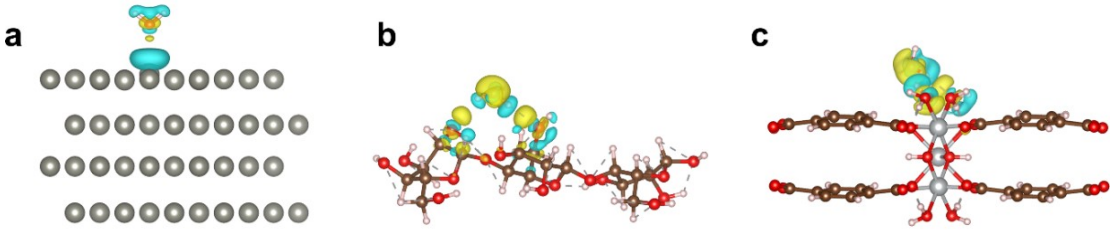

Figure S27. Differential charge density distributions of H_2O with a) Zn, b) CNF and Ni-MOF (yellow and blue colors represent charge accumulation and depletion regions, respectively).

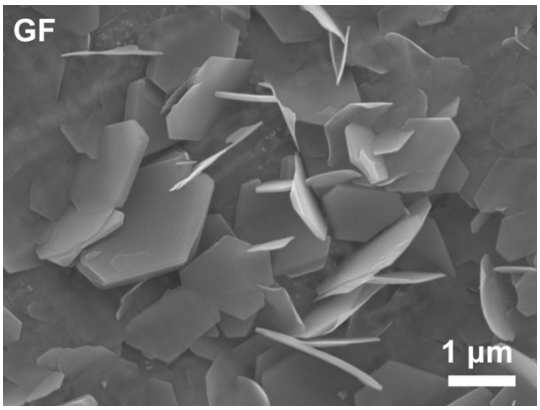

Figure S28. SEM image of the Zn plate with a GF separator after deposition at 1 mA cm^{-2}, 1mAh cm^{-2}, with mixed electrolyte.

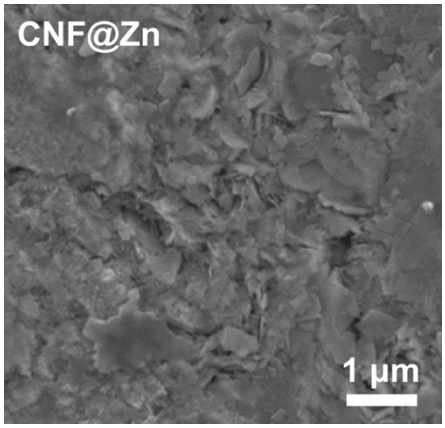

Figure S29. SEM image of CNF@Zn after 50 h of cycling at 1 mA cm^{-2}, 1mAh cm^{-2}, with mixed electrolyte.

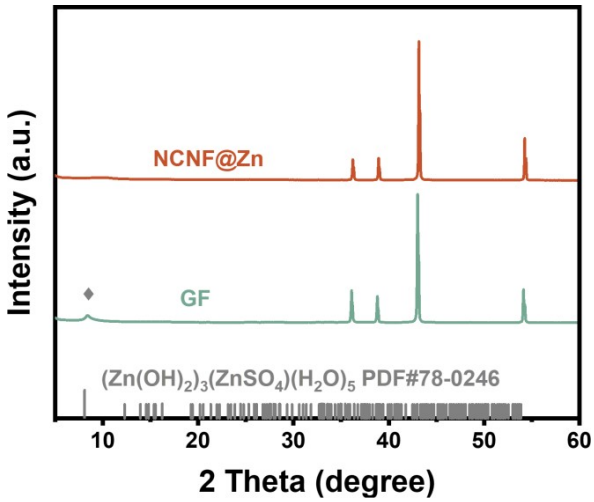

Figure S30. XRD patterns of the NCNF@Zn and bare Zn anodes after deposition at 1 mA cm^{-2}, 1mAh cm^{-2}, with mixed electrolyte.

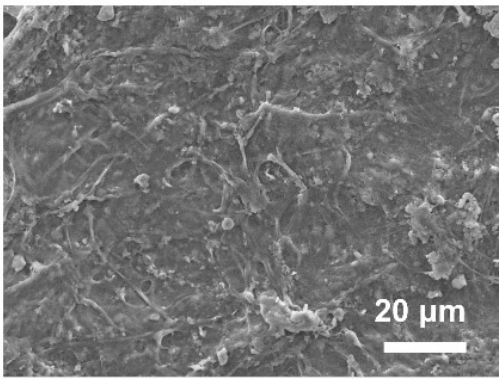

Figure S31. SEM image of NCNF@Zn after cycling for 50 h at 5 mA cm^{-2} and 5 mAh cm^{-2}.

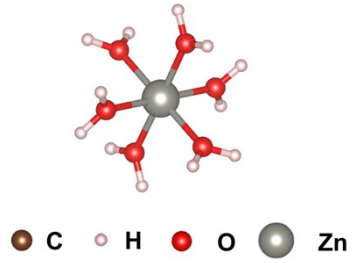

Figure S32. Solvated structure of Zn^{2+}.

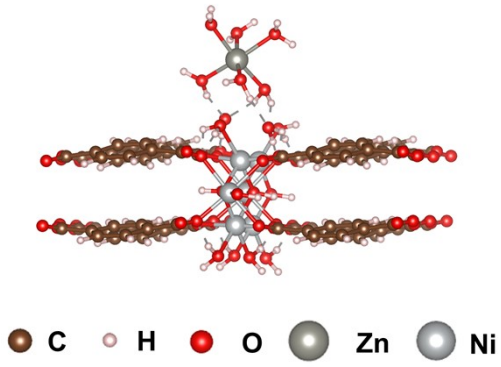

Figure S33. Solvated structure of Zn^{2+} on the surface of Ni-MOF.

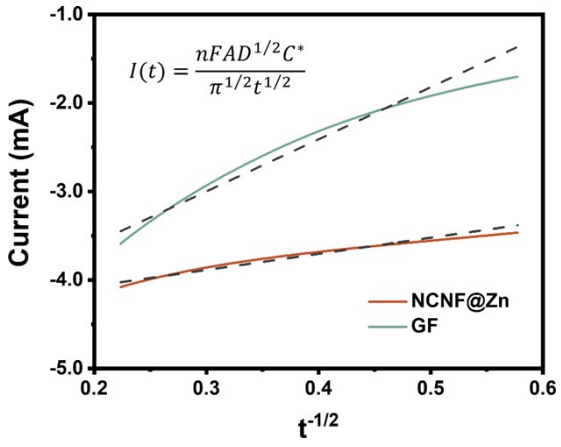

Figure S34. Correlation of the chronoamperometry curve of NCNF@Zn and GF by the Cottrell equation.

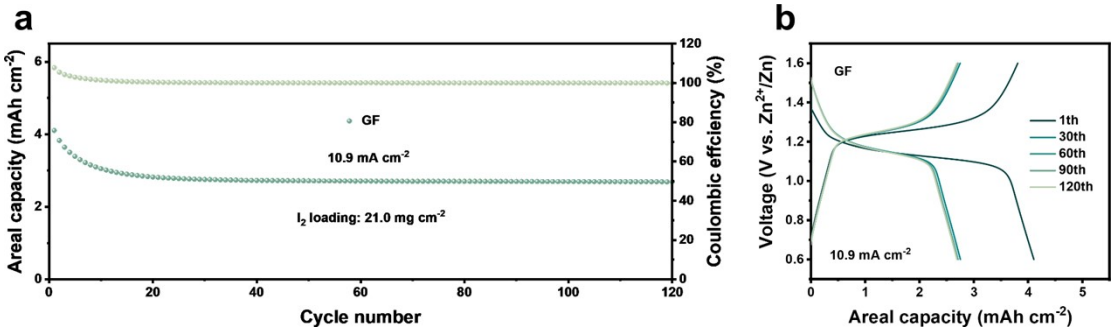

Figure S35. a) Cycling performance and b) corresponding GCD profiles of GF-based battery with a high I_2 mass-loading of 21.0 mg cm^{-2} at 10.9 mA cm^{-2}.

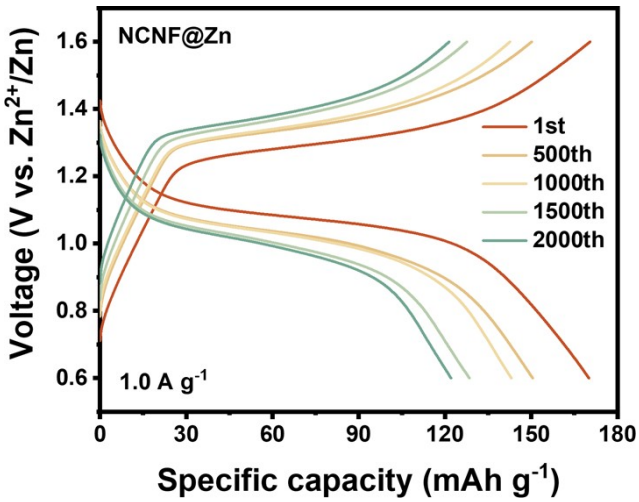

Figure S36. Selected GCD profiles of the flexible separator-free Zn-I_2 pouch cell with NCNF@Zn at 1.0 A g^{-1}.

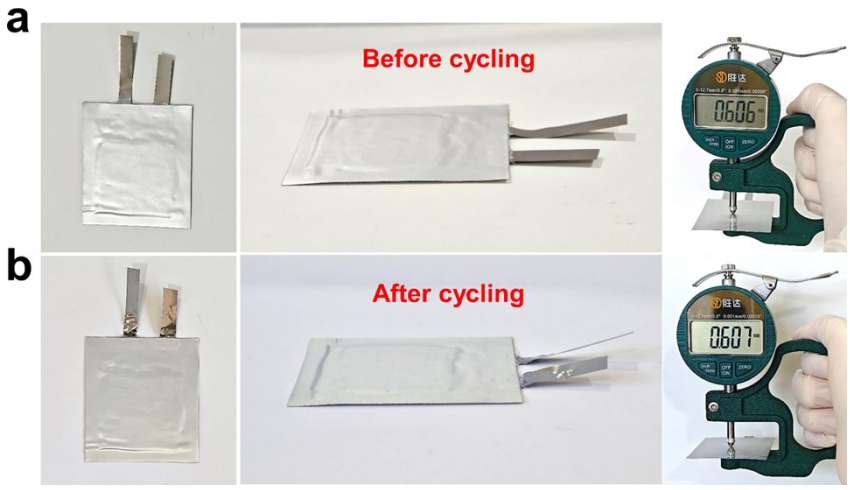

Figure S37. Optical images and thickness variation of the I_2||NCNF@Zn pouch cell a) before and b) after cycling at 1 A g^{-1} for 200 cycles.

Figure S38. Applications of the flexible separator-free pouch cell.

Table S1. Comparison of the separator-free NCNF@Zn battery with reported aqueous Zn–I_2 batteries.

	Current density /mA g^{-1}	Specific capacity /mAh g^{-1}	Cycles	Separator thickness /μm	Reference
Zn-BTC	1920	85.1	6000	＞200	[10]
HT-Zn	4000	90.0	1500	＞200	[11]
Zn@Sn-ZnF_2	2000	96.0	20000	＞200	[12]
SC-PPSZn	3200	84.6	6000	＞200	[13]
LS/I_2	5000	88.0	12000	＞200	[14]
CTS	200	144.1	1500	＞200	[15]
PT@GF	1000	139.9	10000	＞200	[16]
PTCC900@I_2	500	100.0	3000	＞200	[17]
MPC/I_2	1000	112.0	2000	100	[18]
I-BCHP	300	70.0	800	＞200	[19]
CCH	2110	145.0	22000	＞200	[20]
NCNF@Zn	**1000**	**158.2**	**2300**	**24**	**This work**
NCNF@Zn	**5000**	**135.5**	**43000**	**24**	**This work**

Table S2. The Bader charge values of atoms surrounding the I atom in CNF.

CNF- I_3^-	Valence electrons	Total charge	Bader
I1	7	7.33	0.33
O1	6	7.19	1.19
H1	1	0.98	-0.02
H2	1	0.97	-0.03
H3	1	0.35	-0.65
C1	4	3.53	-0.47

Table S3. The Bader charge values of atoms surrounding the I atom in NCNF.

NCNF-I_3^-	Valence electrons	Total charge	Bader
I1	7	7.29	0.29
O1	6	7.13	1.13
H1	1	0.93	-0.07
H2	1	0.92	-0.08
H3	1	0.40	-0.60
C1	4	3.60	-0.40

Table S4. Performance comparison of coin-type Zn-I_2 Batteries.

	Current density /mA cm^{-2}	Areal capacity /mAh cm^{-2}	Reference
LA133	1.56	0.87	[21]
NC-Co/ZnI_2	4.33	2.21	[22]
BBAS	5.06	1.77	[23]
NP-HPC	1.33	1.64	[24]
PVA/CNT	2.0	3.70	[25]
ZMT-ZOF	8.0	0.28	[26]
PEO/PVDF/CD-Si	1.0	0.29	[27]
NCNF@Zn	**10.9**	**4.06**	**This work**

Table S5. Volume calculation of the I_2||NCNF@Zn pouch cell.

Cell components	Length /mm	Width /mm	Thickness /mm	Volume /L
NCNF@Zn anode	24	24	0.060×1 piece	3.46×10^{-5}
I_2 cathode	20	20	0.341×1 piece	1.36×10^{-4}
Aluminum-plastic film	38	38	0.104×2 pieces	3.00×10^{-4}
Total volume (L)	4.71×10^{-4}			

Based on the measured discharge energy of 9.01×10^{-3} Wh and the total device volume of 4.71×10^{-4} L, the volumetric energy density was calculated as following:

$$Energy\ density\ of\ the\ pouch\ cell = \frac{9.01 \times 10^{-3}}{4.71 \times 10^{-4}} = 19.13\ Wh\ L^{-1} \#(6)$$

References

1 J. Cao, D. Zhang, R. Chanajaree, D. Luo, X. Yang, X. Zhang and J. Qin, *Chem. Eng. J.*, 2024, **480**.

2 Z. Wang, Y. Wang, B. Py, A. Maradesa, J. Liu, T. H. Wan, M. Saccoccio and F. Ciucci, *ACS Electrochemistry*, 2025, **1**, 2680-2689.

3 T. H. Wan, M. Saccoccio, C. Chen and F. Ciucci, *Electrochim. Acta*, 2015, **184**, 483-499.

4 G. Kresse and J. Furthmüller, *Phys. Rev. B*, 1996, **54**, 11169-11186.

5 J. P. Perdew, K. Burke and M. Ernzerhof, *Phys. Rev. Lett.*, 1996, **77**, 3865-3868.

6 G. Kresse and D. Joubert, *Phys. Rev. B*, 1999, **59**, 1758-1775.

7 P. E. Blöchl, *Phys. Rev. B*, 1994, **50**, 17953-17979.

8 S. Grimme, J. Antony, S. Ehrlich and H. Krieg, *The Journal of Chemical Physics*, 2010, **132**, 154104.

9 G. Henkelman, B. P. Uberuaga and H. Jónsson, *The Journal of Chemical Physics*, 2000, **113**, 9901-9904.

10 H. Yang, Y. Qiao, Z. Chang, H. Deng, P. He and H. Zhou, *Adv. Mater.*, 2020, **32**, 2004240.

11 B. Ren, S. Hu, A. Chen, X. Zhang, H. Wei, J. Jiang, G. Chen, C. Zhi, H. Li and Z. Liu, *Adv. Energy Mater.*, 2023, **14**, 2302970.

12 G. Wang, Q. Yao, J. Dong, W. Ge, N. Wang, Z. Bai, J. Yang and S. Dou, *Adv. Energy Mater.*, 2023, **14**, 2303221.

13 L. Zhang, J. Huang, H. Guo, L. Ge, Z. Tian, M. Zhang, J. Wang, G. He, T. Liu, J. Hofkens, D. J. L. Brett and F. Lai, *Adv. Energy Mater.*, 2023, **13**, 2203790.

14 Z. Chen, J. Zhang, C. Zhou, S. Guo, D. Wu, Z. Zhao, Z. Wang, J. Li, Z. Xing, P. Rao, Z. Kang, X. Tian and X. Shi, *Adv. Energy Mater.*, 2025, **15**, 2404814.

15 J.-L. Yang, H.-H. Liu, X.-X. Zhao, X.-Y. Zhang, K.-Y. Zhang, M.-Y. Ma, Z.-Y. Gu, J.-M. Cao and X.-L. Wu, *J. Am. Chem. Soc.*, 2024, **146**, 6628-6637.

16 W. Yuan, X. Qu, Y. Wang, X. Li, X. Ru, D. Jia, L. Zhao, Y. Hou, J. Shen, Z.

Shen and N. Zhang, *Energy Storage Mater.*, 2025, **76**, 104130.

17 Y. Wu, Y. Qian, C. Huang, Y. Zhang, Y. Yang, A. Hu, Q. Tang and X. Chen, *Electrochim. Acta*, 2023, **460**, 142593.

18 Y. Hou, F. Kong, Z. Wang, M. Ren, C. Qiao, W. Liu, J. Yao, C. Zhang and H. Zhao, *J. Colloid Interface Sci.*, 2023, **629**, 279-287.

19 J. Xu, W. Ma, L. Ge, M. Ren, X. Cai, W. Liu, J. Yao, C. Zhang and H. Zhao, *J. Alloys Compd.*, 2022, **912**, 165151.

20 J. L. Yang, T. Xiao, T. Xiao, J. Li, Z. Yu, K. Liu, P. Yang and H. J. Fan, *Adv. Mater.*, 2024, **36**, 2313610.

21 K. Wang, H. Li, Z. Xu, Y. Liu, M. Ge, H. Wang, H. Zhang, Y. Lu, J. Liu, Y. Zhang, Y. Tang and S. Chen, *Adv. Energy Mater.*, 2024, **14**, 2304110.

22 J. Ma, A. Azizi, E. Zhang, H. Zhang, A. Pan and K. Lu, *Chem. Sci.*, 2024, **15**, 4581-4589.

23 Y. Liu, F. Li, J. Hao, H. Li, S. Zhang, J. Mao, T. Zhou, R. Wang, L. Zhang and C. Zhang, *Adv. Funct. Mater.*, 2024, **34**, 2400517.

24 Y. Hou, L. Wei, N. Sun, D. Yu and G. Zhao, *J. Storage Mater.*, 2025, **120**, 116495.

25 D. Yin, B. Li, L. Zhao, N. Gao, Y. Zhang, J. Feng, X. Cui, C. Xiao, Y. Su, K. Xi, S. Ding and H. Zhao, *Angew. Chem. Int. Ed.*, 2025, **64**, e202418069.

26 H. Xu, R. Zhang, D. Luo, J. Wang, H. Dou, X. Zhang and G. Sun, *ACS Nano*, 2023, **17**, 25291-25300.

27 Y. Su, X. Wang, M. Zhang, H. Guo, H. Sun, G. Huang, D. Liu and G. Zhu, *Angew. Chem. Int. Ed.*, 2023, **62**, e202308182.